Letter | Editors' Suggestion

Bulk and surface uniformity of magnetic and electronic structures in epitaxial W/Mn_3Sn/MgO films revealed by fluorescence- and electron-yield x-ray magnetic circular dichroism

Shoya Sakamoto,[1,*] Tomoya Higo,[1,2,3] Yoshinori Kotani,[4] Hidetoshi Kosaki,[1] Tetsuya Nakamura,[4,5] Satoru Nakatsuji,[2,1,6,7,3] and Shinji Miwa[1,6,3,†]

[1]*The Institute for Solid State Physics, The University of Tokyo, Kashiwa, Chiba 277-8581, Japan*
[2]*Department of Physics, The University of Tokyo, Bunkyo, Tokyo 113-0033, Japan*
[3]*CREST, Japan Science and Technology Agency (JST), Kawaguchi, Saitama 332-0012, Japan*
[4]*Japan Synchrotron Radiation Research Institute (JASRI), Sayo, Hyogo 679-5198, Japan*
[5]*International Center for Synchrotron Radiation Innovation Smart, Tohoku University, Sendai, Miyagi 980-8572, Japan*
[6]*Trans-scale Quantum Science Institute, The University of Tokyo, Bunkyo, Tokyo 113-0033, Japan*
[7]*Institute for Quantum Matter and Department of Physics and Astronomy, Johns Hopkins University, Baltimore, Maryland 21218, USA*

(Received 13 May 2024; revised 5 August 2024; accepted 7 August 2024; published 29 August 2024)

The chiral kagome antiferromagnet Mn_3Sn has drawn extensive attention for its robust ferromagneticlike responses despite minimal magnetization, and the fabrication of epitaxial W/Mn_3Sn bilayer has unveiled unique spintronics functionalities. However, it remains unclear whether the chiral antiferromagnetic order extends throughout the Mn_3Sn layer in these multilayers. Here, we perform x-ray magnetic circular dichroism measurements on a Mn_3Sn $[1\bar{1}00]$ epitaxial thin film grown on a W underlayer and capped with an MgO overlayer, utilizing both the bulk-sensitive fluorescence-yield mode and the surface-sensitive electron-yield mode. Our analysis reveals that the x-ray absorption spectroscopy and x-ray magnetic circular dichroism (XMCD) spectra obtained from each mode exhibit remarkable congruence, suggesting uniform electronic structures across the entire film thickness and the absence of ferromagnetic inclusions. Furthermore, the XMCD hysteresis loop obtained with the fluorescence-yield mode exhibits a more squarelike profile compared to those obtained with the electron-yield mode and magneto-optical Kerr effect. This indicates minimal domain pinning centers in the bulk region or near the bottom W/Mn_3Sn interface. These findings underscore the intrinsic nature of spin-torque-related phenomena observed in previous studies, affirming their association with the chiral antiferromagnetic spin structure of Mn_3Sn.

DOI: 10.1103/PhysRevB.110.L060412

Introduction. Utilizing antiferromagnets as active components in spintronics devices holds great promise due to their potential for high-speed operation, robustness against magnetic field perturbations, and absence of stray magnetic fields [1–7]. Among the various candidate materials, $D0_{19}$-ordered Mn_3Sn with an inverse triangular spin structure has emerged as a focal point of research due to its pronounced ferromagneticlike behaviors, including anomalous Hall effect [8,9], anomalous Nernst effect [10,11], and magneto-optical Kerr effect [12]. These behaviors stem from the presence of Weyl node pairs in momentum space with strong Berry curvature [13,14].

Recent advancements in epitaxial Mn_3Sn thin film fabrication [15,16] have showcased unique spintronics functionalities such as binary full switching of octupole polarization [17], tunneling magnetoresistance effect [18], and the chiral spin rotation [19]. Despite these demonstrations, it remains unclear whether the chiral antiferromagnetic order is realized throughout the film from the bottom to top interfaces. This uncertainty is critical for understanding spin-torque induced phenomena, which occur through interfaces.

To clarify this uncertainty, we perform x-ray magnetic circular dichroism (XMCD) measurements on an epitaxial Mn_3Sn/W bilayer thin film employing both surface-sensitive total-electron-yield (TEY) and bulk-sensitive partial-fluorescence-yield (PFY) modes. While XMCD is usually absent for antiferromagnetic materials, the emergence of XMCD in the inverse triangular spin structure was demonstrated both theoretically [20–23] and experimentally [24,25] recently, and XMCD is becoming a powerful tool to characterize the octupole polarization.

Methods. The Mn_3Sn thin film, with the kagome planes standing normal to the sample surface was grown on a single-crystalline MgO(110) substrate with a W seed layer by molecular beam epitaxy [17,24]. Figure 1(a) illustrates the schematic sample structure: MgO(110) substrate/W (7 nm)/Mn_3Sn (30 nm)/MgO (3 nm). The substrate underwent annealing at 800 °C for 10 min before the deposition. The W layer was grown at the substrate temperature of 300 °C with a growth rate of 0.1 Å/s, followed by annealing at 800 °C for 10 min to obtain a flat surface. For Mn_3Sn deposition, a 5-nm-thick Mn_3Sn layer was initially grown at a rate of 0.25 Å/s at room temperature and annealed at 350 °C for 10 min. Subsequently, a 25-nm-thick Mn_3Sn layer was grown at a rate of 0.25 Å/s at 260 °C. A 3-nm-thick MgO capping layer was deposited at room temperature, followed by

*Contact author: shoya.sakamoto@issp.u-tokyo.ac.jp
†Contact author: miwa@issp.u-tokyo.ac.jp

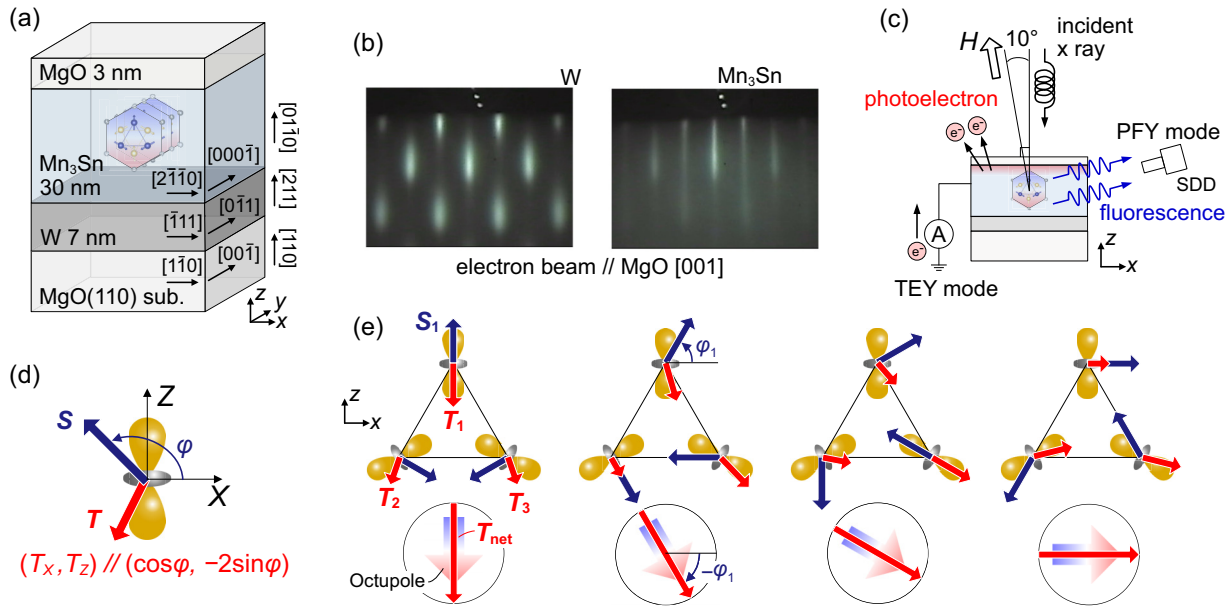

FIG. 1. (a) Schematic representation of the sample structure with cluster magnetic octupoles depicted by hexagons with blue and red gradations. (b) Reflection high-energy electron diffraction patterns for the W seed layer after annealing and the Mn_3Sn layer. (c) Geometry of the XMCD measurements. (d) Spin angular momentum $\boldsymbol{S}$ and magnetic dipole term $\boldsymbol{T}$ for the d_{z^2} orbital. (e) Net magnetic dipole term and octupole polarization in the inverse triangular spin structure.

annealing at 600 °C for 30 min. The actual atomic composition was estimated to be approximately Mn:Sn = 3.07:0.93 by energy dispersive x-ray spectroscopy. Mn and Sn atoms were codeposited using effusion cells, and other layers were grown using the electron-beam evaporation method.

The surface quality of each layer was monitored during deposition using reflection high-energy electron diffraction (RHEED). The RHEED patterns of W and Mn_3Sn layers, taken with electron beams parallel to the [001] direction of the MgO(110) substrate, are depicted in Fig. 1(b). The streaky RHEED patterns are consistent with those reported in a previous study [17], confirming the epitaxial growth of each layer. The RHEED patterns of the MgO capping layer (not shown) suggested that the in-plane orientation of MgO in the capping layer is random. Magnetic properties were characterized using polar magneto-optical Kerr effect (MOKE) with a 660 nm continuous wave laser at room temperature.

X-ray absorption spectroscopy (XAS) and XMCD measurements were conducted at BL-25SU at SPring-8, with the measurements taken at room temperature. The measurement geometry is depicted in Fig. 1(c) [26]. Magnetic fields (H) of up to 1.9 T were applied at a 10° angle from the sample normal, while the x-ray beam impinged perpendicularly to the sample surface. In the TEY mode, a total current compensating for photoelectron loss was measured. For the PFY mode, fluorescence x rays from Mn atoms were selectively detected using a silicon drift detector with energy-resolving capability. The probing depth of TEY and PFY modes are typically a few nm and approximately 100 nm, respectively. Therefore, the TEY mode can probe surface regions while the PFY mode probes the entire 30-nm-thick Mn_3Sn layer.

XMCD signals were measured by reversing the helicity of x rays at a frequency of 1 Hz at each photon energy under a fixed magnetic field. The XAS spectra were obtained as $(\sigma_{R,+H} + \sigma_{L,+H}) + (\sigma_{R,-H} + \sigma_{L,-H})$, and XMCD spectra were obtained as $(\sigma_{R,+H} - \sigma_{L,+H}) - (\sigma_{R,-H} - \sigma_{L,-H})$, where $\sigma_{R/L,\pm H}$ denotes the absorption coefficient measured with right- or left-circularly polarized x rays under positive or negative magnetic fields. The XMCD hysteresis loops were obtained by recording XMCD signals at each magnetic field at a fixed photon energy. Here, XMCD signals are normalized to XAS signals at each magnetic field and are symmetrized using sweeps from positive to negative magnetic fields and vice versa.

Here, let us explain the origin of XMCD signals in Mn_3Sn with the inverse triangular spin structure. XMCD signals stem not only from the spin angular momentum $\boldsymbol{S}$ but also from magnetic dipole term $\boldsymbol{T} = \boldsymbol{S} - 3(\boldsymbol{S}\cdot\hat{\boldsymbol{r}})\hat{\boldsymbol{r}}$, where $\boldsymbol{S}$ and $\hat{\boldsymbol{r}}$ denote the spin angular momentum and unit electron position operators, respectively [27,28]. The magnetic dipole term in the d_{z^2} orbitals in X-Z coordinates is illustrated in Fig. 1(d) as an example and can be expressed as $(T_X, T_Z) = \frac{|\boldsymbol{S}|}{7}(\cos\phi, -2\sin\phi)$, with ϕ denoting the angle of spin with respect to the X axis [21]. Utilizing this relationship, it can be generally shown that the net magnetic dipole term $\boldsymbol{T}_{\rm net}$ in the inverse triangular spin structure rotates oppositely to each Mn spin without changing its magnitude [23], as depicted in Fig. 1(e). Since the octupole polarization also rotates oppositely to the spins [29] in a manner akin to the dipole term [30], XMCD serves as an effective means to probe the projected octupole polarization along the incident x-ray direction.

Results & Discussion. Figure 2(a) displays XAS spectra obtained using both the TEY and PFY modes. The spectra are normalized to unity at the L_3 edge maximum. In the PFY spectrum, relatively large intensities are observed at the L_2

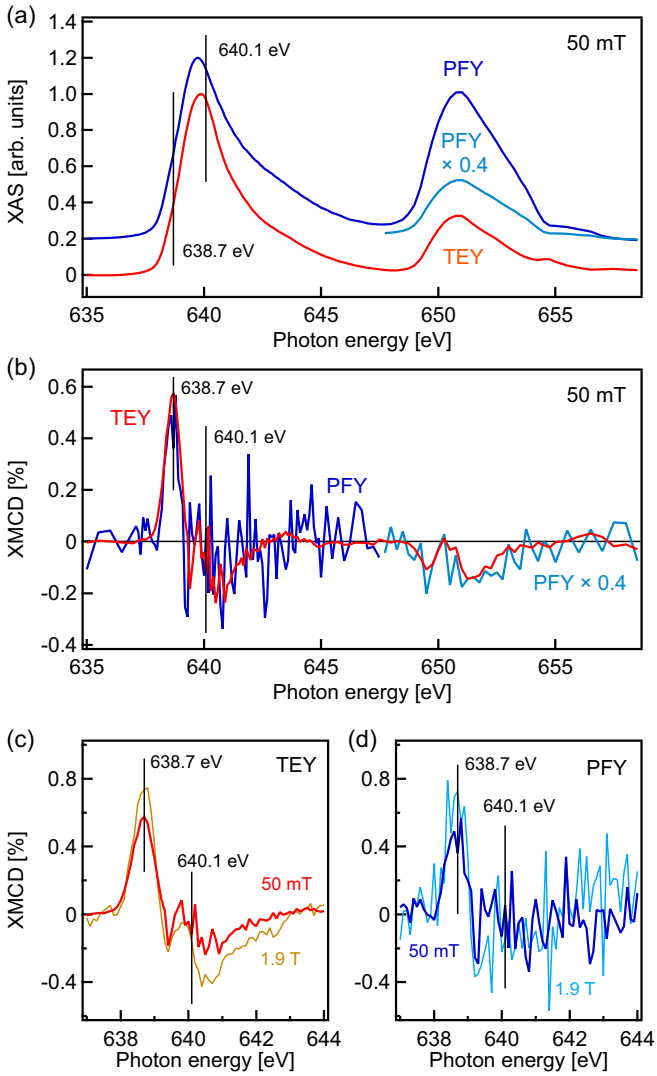

FIG. 2. (a) XAS and (b) XMCD spectra taken with TEY and PFY modes. Each XAS and XMCD spectrum is normalized by the XAS L_3 edge maximum. As PFY spectra are distorted by the self-absorption effect, the PFY spectrum around the L_2 edge is separately scaled by a factor of 0.4. (c) TEY L_3 edge and (d) PFY L_3 edge XMCD spectra acquired with magnetic fields of 50 mT and 1.9 T.

edge due to the self-absorption effect [31]. To facilitate better comparison, the PFY L_2 edge peak is separately scaled down by a factor of 0.4, as indicated by the light-blue curves in Fig. 2(a). The spectra exhibit single broad peaks for each Mn L_2 and L_3 edge and do not show multiplet features. Such a line shape is typical of metallic compounds, and weak shoulder features observed in previous studies [24,25] were likely extrinsic, originating from Mn oxides formed at the surface. Note that the weak peak feature around 655 eV arises from Mg K-edge absorption from higher-order x rays with doubled photon energy. The agreement in line shape between the TEY and PFY spectra suggests that the electronic structure does not vary significantly between the bulk and surface regions.

Figure 2(b) shows XMCD spectra obtained using both the TEY and PFY modes at a magnetic field of 50 mT. Initially, a magnetic field of ±1.9 T was applied and then reduced

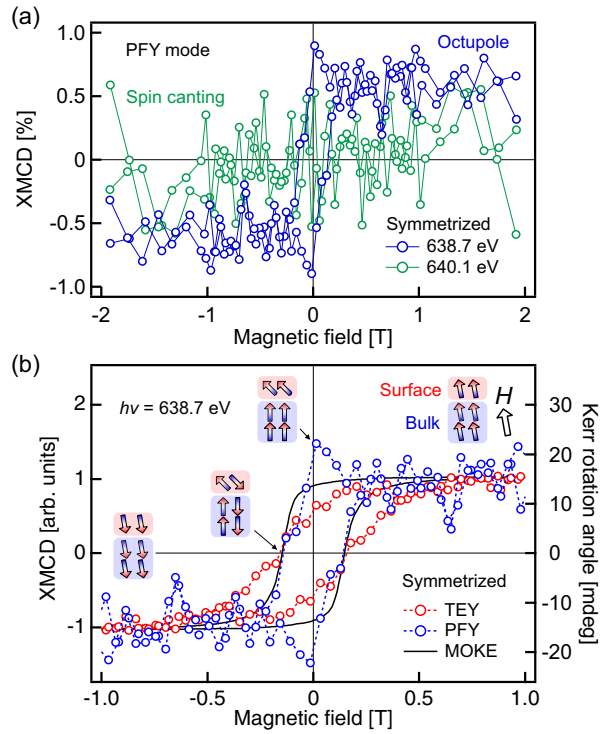

FIG. 3. (a) PFY XMCD hysteresis loops obtained with photon energies of 638.7 eV and 640.1 eV, corresponding to octupole and spin-canting components, respectively [24]. (b) TEY and PFY XMCD hysteresis loops obtained with a photon energy of 638.7 eV. A hysteresis loop measured with MOKE is also included for comparison. The proposed magnetization process for bulk and surface regions are also schematically illustrated in the insets.

to ±50 mT to investigate the remanent state. The L_2 edge peak is scaled down by a factor of 0.4 to correct for the self-absorption effect. Consistent with the XAS spectra, both the TEY and PFY XMCD spectra closely resemble each other, suggesting that not only the electronic structure but also the magnetic structure remains consistent throughout the entire Mn_3Sn layer. This consistency indicates the absence of significant unwanted second phases, such as ferromagnetic W-Mn-Sn intermetallic compounds, near the bottom Mn_3Sn/W interface.

The XMCD intensity (∼0.6%) of the positive peak at 638.7 eV is approximately three times stronger than that reported in a previous study (∼0.2%) [24]. This is likely due to the higher quality of the present sample compared to the sample studied in the previous research. In fact, the saturation Kerr rotation angle [∼15 mdeg, Fig. 3(a)] was three times larger than that reported in the previous study (∼5 mdeg).

Figures 2(c) and 2(d) depict the magnetic field dependence of the TEY and PFY XMCD spectra at the Mn L_3 edge, respectively. The intensity of the TEY XMCD spectrum increases with increasing magnetic fields. Importantly, the XMCD line shape remains almost unchanged by magnetic fields, indicating the absence of significant ferromagnetic, superparamagnetic, or paramagnetic second phases, which would emerge or grow as the magnetic field increases. Furthermore, it also suggests the absence of significant spin canting.

To delve deeper into the magnetic field dependence, we conducted magnetic field sweep measurements with fixed photon energies and obtained XMCD hysteresis loops. Figure 3(a) displays the PFY hysteresis loops measured with photon energies of 638.7 eV and 640.1 eV. Here, 638.7 eV and 640.1 eV correspond to the octupole and spin-canting components, respectively [24]. It was observed that the spin-canting component is almost nonexistent within the accuracy of the measurements.

Figure 3(b) presents the XMCD hysteresis loops acquired with both the TEY and PFY modes at a photon energy of 638.7 eV, corresponding to the strong pre-edge positive peak as marked by the vertical lines in Fig. 2. A hysteresis loop measured with MOKE is included for comparison. The coercive fields of approximately 150 mT are consistent among the TEY, PFY and MOKE hysteresis loops, aligning with those reported in a previous study [17]. The PFY XMCD signals display a slight increase as magnetic fields approach zero from higher magnetic fields. This observation suggests that the octupole polarization points toward the out-of-plane or the x-ray incidence direction from the magnetic field direction, owing to perpendicular magnetic anisotropy induced by tensile epitaxial strain in the Mn_3Sn $[2\bar{1}\bar{1}0]$ direction [17].

In contrast, the TEY hysteresis curve exhibits opposite behavior, decreasing as magnetic fields approach zero from higher magnetic fields. Moreover, achieving saturation of the octupole polarization in the TEY hysteresis loop requires higher magnetic fields. Spin canting or other magnetic inclusions cannot account for this behavior, as they would yield negative XMCD signals that decrease as magnetic fields increase. Therefore, we infer that perpendicular uniaxial magnetic anisotropy diminishes only near the MgO interface, possibly due to relaxed strain or influence from MgO interface, and the sixfold, fourfold, or in-plane magnetic anisotropy becomes dominant, thereby tilting the octupole polarization away from the surface normal. This explanation aligns with the consistent line shapes observed between the TEY and PFY spectra. Note that the inherent sixfold magnetic anisotropy alone may not fully explain the ∼60% reduction of the remanence octupole polarization from the saturation value, as the ∼60% reduction corresponds to the octupole polarization angle of ∼50 degrees from the surface normal. The identical coercive fields observed between the TEY and PFY hysteresis loops eliminate the possibility of other magnetic inclusions and suggest weak magnetic coupling between the surface and bulk regions. The magnetization process described above is illustrated in the insets of Fig. 3(b).

The absence of any magnetic inclusions and the observed sharp squarelike PFY hysteresis loops suggest that the recently observed spin-torque related phenomena [17,19], which occurs at the Mn_3Sn/W interfaces, and tunneling magnetoresistance [18] happening at the Mn_3Sn/MgO interfaces are intrinsic, reflecting the chiral antiferromagnetic order. The present findings indicate that achieving high-quality Mn_3Sn/W bilayers is feasible and lay the foundation for advancing antiferromagnetic spintronics based on noncollinear antiferromagnets.

Conclusion. In this Letter, we investigated the uniformity of the magnetic structure of a Mn_3Sn $[1\bar{1}00]$ epitaxial thin film from the bottom to top interfaces using XMCD measurements with both bulk-sensitive partial-fluorescence-yield mode and surface-sensitive total-electron-yield modes. The XAS and XMCD spectra obtained from each mode exhibit nearly identical characteristics, indicating uniform electronic and magnetic structures throughout the entire film thickness and the absence of other magnetic inclusions. Furthermore, the XMCD hysteresis loop acquired with the fluorescence-yield mode displays a more squarelike profile compared to those obtained with the electron-yield mode and magneto-optical Kerr effect. This suggests minimal domain pinning centers in the bulk region or near the bottom W/Mn_3Sn interface. These findings underscore the intrinsic nature of spin-torque-related phenomena observed in previous studies and provide a solid foundation for future investigations.

Acknowledgments. The XMCD experiments were performed at the BL25SU of SPring-8 with the approval of the Japan Synchrotron Radiation Research Institute (JASRI) (Proposal No. 2022A1072). This work was supported by JSPS KAKENHI (No. JP22H00290, No. JP22H04964, No. JP23H01833, and No. JP24H02234), JST CREST (JPMJCR18T3), JST-Mirai Program (JPMJMI20A1), MEXT Initiative to Establish Next-Generation Novel Integrated Circuit Centers (X-NICS) (No. JPJ011438), and Spintronics Research Network of Japan (Spin-RNJ). Institute for Quantum Matter, an Energy Frontier Research Center was funded by DOE, Office of Science, Basic Energy Sciences under Award No. DE-SC0019331.

[1] T. Jungwirth, X. Marti, P. Wadley, and J. Wunderlich, Antiferromagnetic spintronics, Nat. Nanotechnol. **11**, 231 (2016).

[2] V. Baltz, A. Manchon, M. Tsoi, T. Moriyama, T. Ono, and Y. Tserkovnyak, Antiferromagnetic spintronics, Rev. Mod. Phys. **90**, 015005 (2018).

[3] T. Jungwirth, J. Sinova, A. Manchon, X. Marti, J. Wunderlich, and C. Felser, The multiple directions of antiferromagnetic spintronics, Nat. Phys. **14**, 200 (2018).

[4] L. Šmejkal, Y. Mokrousov, B. Yan, and A. H. MacDonald, Topological antiferromagnetic spintronics, Nat. Phys. **14**, 242 (2018).

[5] L. Šmejkal, A. H. MacDonald, J. Sinova, S. Nakatsuji, and T. Jungwirth, Anomalous Hall antiferromagnets, Nat. Rev. Mater. **7**, 482 (2022).

[6] S. Nakatsuji and R. Arita, Topological magnets: Functions based on Berry phase and multipoles, Annu. Rev. Condens. Matter Phys. **13**, 119 (2022).

[7] J. Han, R. Cheng, L. Liu, H. Ohno, and S. Fukami, Coherent antiferromagnetic spintronics, Nat. Mater. **22**, 684 (2023).

[8] S. Nakatsuji, N. Kiyohara, and T. Higo, Large anomalous Hall effect in a non-collinear antiferromagnet at room temperature, Nature (London) **527**, 212 (2015).

[9] Y. Zhang, Y. Sun, H. Yang, J. Železný, S. P. P. Parkin, C. Felser, and B. Yan, Strong anisotropic anomalous Hall effect and spin Hall effect in the chiral antiferromagnetic compounds Mn_3X (X = Ge, Sn, Ga, Ir, Rh, and Pt), Phys. Rev. B **95**, 075128 (2017).

[10] M. Ikhlas, T. Tomita, T. Koretsune, M.-T. Suzuki, D. Nishio-Hamane, R. Arita, Y. Otani, and S. Nakatsuji, Large anomalous Nernst effect at room temperature in a chiral antiferromagnet, Nat. Phys. **13**, 1085 (2017).

[11] X. Li, L. Xu, L. Ding, J. Wang, M. Shen, X. Lu, Z. Zhu, and K. Behnia, Anomalous Nernst and Righi-Leduc effects in Mn_3Sn: Berry curvature and entropy flow, Phys. Rev. Lett. **119**, 056601 (2017).

[12] T. Higo, H. Man, D. B. Gopman, L. Wu, T. Koretsune, O. M. J. van 't Erve, Y. P. Kabanov, D. Rees, Y. Li, M.-T. Suzuki, S. Patankar, M. Ikhlas, C. L. Chien, R. Arita, R. D. Shull, J. Orenstein, and S. Nakatsuji, Large magneto-optical Kerr effect and imaging of magnetic octupole domains in an antiferromagnetic metal, Nat. Photon. **12**, 73 (2018).

[13] K. Kuroda, T. Tomita, M. T. Suzuki, C. Bareille, A. A. Nugroho, P. Goswami, M. Ochi, M. Ikhlas, M. Nakayama, S. Akebi, R. Noguchi, R. Ishii, N. Inami, K. Ono, H. Kumigashira, A. Varykhalov, T. Muro, T. Koretsune, R. Arita, S. Shin *et al.*, Evidence for magnetic Weyl fermions in a correlated metal, Nat. Mater. **16**, 1090 (2017).

[14] H. Yang, Y. Sun, Y. Zhang, W.-J. Shi, S. S. P. Parkin, and B. Yan, Topological Weyl semimetals in the chiral antiferromagnetic materials Mn_3 Ge and Mn_3 Sn, New J. Phys. **19**, 015008 (2017).

[15] Y. You, X. Chen, X. Zhou, Y. Gu, R. Zhang, F. Pan, and C. Song, Anomalous Hall effect–like behavior with in-plane magnetic field in noncollinear antiferromagnetic Mn_3 Sn films, Adv. Electron. Mater. **5**, 1800818 (2019).

[16] J. Yoon, Y. Takeuchi, R. Itoh, S. Kanai, S. Fukami, and H. Ohno, Crystal orientation and anomalous Hall effect of sputter-deposited non-collinear antiferromagnetic Mn_3 Sn thin films, Appl. Phys. Express **13**, 013001 (2020).

[17] T. Higo, K. Kondou, T. Nomoto, M. Shiga, S. Sakamoto, X. Chen, D. Nishio-Hamane, R. Arita, Y. Otani, S. Miwa, and S. Nakatsuji, Perpendicular full switching of chiral antiferromagnetic order by current, Nature (London) **607**, 474 (2022).

[18] X. Chen, T. Higo, K. Tanaka, T. Nomoto, H. Tsai, H. Idzuchi, M. Shiga, S. Sakamoto, R. Ando, H. Kosaki, T. Matsuo, D. Nishio-Hamane, R. Arita, S. Miwa, and S. Nakatsuji, Octupole-driven magnetoresistance in an antiferromagnetic tunnel junction, Nature (London) **613**, 490 (2023).

[19] Y. Takeuchi, Y. Yamane, J.-Y. Yoon, R. Itoh, B. Jinnai, S. Kanai, J. Ieda, S. Fukami, and H. Ohno, Chiral-spin rotation of non-collinear antiferromagnet by spin–orbit torque, Nat. Mater. **20**, 1364 (2021).

[20] S. Wimmer, S. Mankovsky, J. Minár, A. N. Yaresko, and H. Ebert, Magneto-optic and transverse-transport properties of noncollinear antiferromagnets, Phys. Rev. B **100**, 214429 (2019).

[21] Y. Yamasaki, H. Nakao, and T.-H. Arima, Augmented magnetic octupole in kagomé 120-degree antiferromagnets detectable via X-ray magnetic circular dichroism, J. Phys. Soc. Jpn. **89**, 083703 (2020).

[22] N. Sasabe, M. Kimata, and T. Nakamura, Presence of X-ray magnetic circular dichroism signal for zero-magnetization antiferromagnetic state, Phys. Rev. Lett. **126**, 157402 (2021).

[23] G. van der Laan, Determination of spin chirality using X-ray magnetic circular dichroism, Phys. Rev. B **104**, 094414 (2021).

[24] S. Sakamoto, T. Higo, M. Shiga, K. Amemiya, S. Nakatsuji, and S. Miwa, Observation of spontaneous X-ray magnetic circular dichroism in a chiral antiferromagnet, Phys. Rev. B **104**, 134431 (2021).

[25] M. Kimata, N. Sasabe, K. Kurita, Y. Yamasaki, C. Tabata, Y. Yokoyama, Y. Kotani, M. Ikhlas, T. Tomita, K. Amemiya, H. Nojiri, S. Nakatsuji, T. Koretsune, H. Nakao, T. Arima, and T. Nakamura, X-ray study of ferroic octupole order producing anomalous Hall effect, Nat. Commun. **12**, 5582 (2021).

[26] T. Nakamura, T. Muro, F. Guo, T. Matsushita, T. Wakita, T. Hirono, Y. Takeuchi, and K. Kobayashi, Development of a soft X-ray magnetic circular dichroism spectrometer using a 1.9 T electromagnet at BL25SU of SPring-8, J. Electron Spectrosc. Relat. Phenom. **144-147**, 1035 (2005).

[27] J. Stöhr and H. König, Determination of spin- and orbital-moment anisotropies in transition metals by angle-dependent X-ray magnetic circular dichroism, Phys. Rev. Lett. **75**, 3748 (1995).

[28] J. Stöhr, Exploring the microscopic origin of magnetic anisotropies with X-ray magnetic circular dichroism (XMCD) spectroscopy, J. Magn. Magn. Mater. **200**, 470 (1999).

[29] J.-Y. Yoon, P. Zhang, C.-T. Chou, Y. Takeuchi, T. Uchimura, J. T. Hou, J. Han, S. Kanai, H. Ohno, S. Fukami, and L. Liu, Handedness anomaly in a non-collinear antiferromagnet under spin–orbit torque, Nat. Mater. **22**, 1106 (2023).

[30] The net dipole term can be explicitly calculated as $7\boldsymbol{T}_{\mathbf{net}}/|\boldsymbol{S}| = \binom{\cos\phi_1}{-2\sin\phi_1} + R_{2\pi/3}\binom{\cos(\phi_1+2\pi/3)}{-2\sin(\phi_1+2\pi/3)} + R_{4\pi/3}\binom{\cos(\phi_1+4\pi/3)}{-2\sin(\phi_1+4\pi/3)} = \frac{9}{2}(\cos\phi_1, -\sin\phi_1)$, where ϕ_1 represents the angle of the spin at site 1, as shown in Fig. 1(e), and R_θ represents the rotation matrix. The octupole polarization is commonly defined as $\frac{1}{3}M_z[S_1 + R_{\frac{2\pi}{3}}S_2 + R_{\frac{4\pi}{3}}S_3] = (\cos\phi_1, -\sin\phi_1)$, with M_z denoting the mirror operation along the z axis and behaving the same way as the net magnetic dipole term.

[31] L. Tröger, D. Arvanitis, K. Baberschke, H. Michaelis, U. Grimm, and E. Zschech, Full correction of the self-absorption in soft-fluorescence extended X-ray-absorption fine structure, Phys. Rev. B **46**, 3283 (1992).